Journal of the European Ceramic Society 17 (1997) 77–84

PII: S0955-2219(96)00073-8
0955-2219/97/$17.00

Microstructural Analysis of Corroded Alumina–Spinel Castable Refractories

P. Korgul,[a] D. R. Wilson[b] & W. E. Lee[a]*

[a]Department of Engineering Materials, University of Sheffield, S1 3JD, UK
[b]Redland Minerals, Hartlepool, TS24 0BY, UK

(Received 27 February 1996; revised version received 11 March 1996; accepted 28 March 1996)

Abstract

Microstructural analysis indicates that the corrosion of alumina–spinel castables by a liquid steel ladle slag involves initial reaction of CaO in the slag with alumina fines in the refractory bond. The slag becomes saturated in CaO and Al_2O_3 and CA_2 is precipitated from it along with other calcium aluminates. The spinel fines and grains in the refractory take up the $MnO/FeO/Fe_2O_3$ from the slag, which becomes silica-rich as CA_2 is precipitated and highly viscous. The thickness of the remnant slag layer on the corroded samples indicates the viscosity of the liquid slag under the test conditions. Further into the refractory CA_6 is formed, firstly crystallized with a tabular morphology in dense regions and then with a similar morphology in more porous regions. Deeper still in the refractory CA_6 takes a whisker/needle habit suggesting some vapour-phase reaction. MgO-rich spinel–alumina castables undergo less corrosion under these conditions as dissolution of MgO leads to a viscous MgO-rich slag which is less corrosive to the Al_2O_3 components of the refractory. © *1996 Elsevier Science Limited.*

1 Introduction

Monolithic refractory castables based on mixtures of Al_2O_3 and 10–25% $MgAl_2O_4$ spinel grain and calcium-aluminate-derived bond are being used increasingly in steel ladles, continuous casting tundishes, degasser snorkels and lances, following recent development of this system.[1–2] The lifetimes of linings made from these castables are limited by their wear rate arising from slag penetration and structural spalling,[3] so that a thorough understanding of the corrosion mechanisms is desirable. Since the slag is the most corrosive component in the melt, its composition has a critical effect on the corrosion mechanism. Unfortunately, slag composition varies greatly between steelworks and even between different batches in the same steelworks, so that a complete model of slag corrosion of a refractory is difficult to achieve. Typical industrial corrosion tests for refractories include dipping tests where a sample is held in the corrosive medium, induction furnace slag tests where the corrosive medium is melted in a refractory-lined induction furnace, crucible tests in which the corrosive medium is melted in a cored-out brick and rotary slag tests where the corrosive medium is melted with an oxy-acetylene flame in a drum rotating about a horizontal axis lined with sections of refractory. Corrosion resistance in the rotary slag test is evaluated based on thickness loss and the depth of penetration. Benefits of this particular method include: (1) corrosion rate can be obtained for several refractories simultaneously, (2) the thermal gradient in the samples can be similar to service conditions and (3) it is a dynamic test with the slag being in motion, i.e. there is an abrasion component to the corrosive wear. These tests, however, are designed to indicate lining lifetimes rather than to give an understanding of the corrosion mechanism. Nonetheless, when used in conjunction with detailed analysis of the slag-attacked regions, an idea of the corrosion mechanism may be obtained.

In alumina–spinel refractories the stoichiometry of the spinel used strongly influences the corrosion behaviour, with alumina-rich spinel addition increasing the resistance to slag penetration and wear.[4–6] Furthermore, the size of the spinel particles added also affects the wear rate, fine particle additions being more effective in resisting corrosion than coarse grain additions. However, spalling resistance is improved with coarse (>0·3 mm) spinel addition[3] since fine additions result in excessive sintering shrinkage and consequent stress, so

*To whom correspondence should be addressed.

that a range of spinel sizes is needed. Results are presented here of detailed analysis of castable microstructures containing spinels with a range of stoichiometries but fixed particle-size distribution. Microstructures are determined before and after slag corrosion testing in an attempt to elucidate the mechanism of corrosive attack by a typical ladle slag composition.

2 Experimental

The castable formulation (Table 1) was chosen to optimize resistance to slag penetration.[7] Four different grades of sintered spinel were used containing 67, 70, 75 and 90 wt% Al_2O_3 respectively, i.e. two substoichiometric and two alumina-rich, the stoichiometric amount of Al_2O_3 in spinel being 71.67 wt%. The spinel was manufactured by sintering to a maximum temperature of 1800°C and came from various suppliers depending on stoichiometry. The 90% alumina spinel was from Alcoa, the 70% from Onoda and the 67 and 75% alumina spinels from Redland Minerals. Additionally, a fifth sample was made as a control containing no spinel, which was replaced with equivalently sized (i.e. 2·36–1·18 and 1·18–0·6 mm) tabular alumina. Batches weighing 7 kg were dry-mixed in a Hobart A120 FM mixer before adding water and wet mixing for 4 min. Water addition of 6·8 wt% was found to give good casting consistency for all aggregates tested. The mixed material was vibration-cast into 100 × 100 × 230 mm stainless steel moulds. Vibration time was 4 min at a frequency of 50 Hz. Samples were wrapped in plastic and cured at room temperature for 24 h. After mould removal samples were rewrapped in plastic and cured at room temperature for a further 24 h. The plastic was discarded and the castable allowed to dry for 24 h. Each block was then dried for 3 days at 110°C. The test blocks were then finally cut to exact size for the rotary slag test without pre-firing.

The rotary slag apparatus used was similar to that in BS1902 section 5.13. The cut samples form the inner lining of a horizontal drum rotating at 5 rev min^{-1}. All castables were given a rotary slag test over 2 days using a synthetic ladle slag with the composition given in Table 2. The lime-rich $CaO–MgO–MnO–Al_2O_3–SiO_2$ slag also contains Fe to simulate the conditions in a ladle slag. The test procedure was also designed to match as closely as possible the conditions in a steel ladle. Slag was added when the furnace had reached the test temperature of 1650°C, spent slag removed and fresh slag added at approximately 1 h intervals over the 2 day period. The furnace was switched off at the end of day 1 and emptied before allowing to cool overnight. On day 2 the furnace was brought up to temperature again and the remelted residual slag from day 1 added. Again, fresh slag was added at hourly intervals. A total of 2·6 kg of slag was added and total time at 1650°C was 12·2 h. The depth of erosion and slag penetration (defined as the depth of discoloration by Fe_2O_3) was determined for cross-sections of each block at 12 mm intervals. This measure of slag penetration is invariably an underestimate since penetration occurs further than the discoloured depth.[8]

Two samples of each formulation were examined: one from the slag–refractory interface and one from the back of the block which provides an example of the unattacked castable microstructure although its temperature for the duration of the test is unknown. Some of the back samples were given a further heat treatment for 40 h at 1650°C in air to determine which changes in the microstructure were simply due to the temperature of the slag test. Standard ceramographic grinding and polishing techniques were used after mounting in resin. All samples were carbon-coated and examined in backscattered and secondary electron imaging mode on a JEOL 6400 or Philips 500 scanning electron microscope (SEM). Energy-dispersive spectroscopy (EDS) was done using a Link eXL system with an ultrathin window detector on the JEOL 6400. Weighted average atomic numbers (Z) of important phases in the microstructures are given in Table 3. Such tables are useful because the higher the value of Z, the brighter the phase appears in a backscattered electron image.

Table 1. Castable formulations

Formulation	*Wt%*
Tabular alumina	
6·3–2·36 mm	25
2·36–1·18	4
1·18–0·6	5
0·6–0	13
–325 mesh	6
Mg aluminate spinel	
3–1 mm	15
1–0 mm	10
Calcined alumina (Alcan RA10)	10
CA cement (Secar 80)	12

Table 2. Composition of rotary test slag

Composition	*Wt%*
CaO	56·8
SiO_2	16·5
MgO	4·4
Al_2O_3	10·7
MnO	5·4
Total iron as Fe	5·9

Table 3. Weighted average atomic numbers and melting temperatures of phases observed

Phase	*Weighted average atomic number*[a]	*Melting/decomposition temperature (°C)*
Al_2O_3	10·65	2050
$MgO.Al_2O_3$	10·58	2135
MgO	10·41	2620
$CaO.2Al_2O_3$	11·93	1750–1765
$CaO.6Al_2O_3$	11·15	1850

[a]Details of how to calculate these values are given in Ref. 9.

3 Results

3.1 Uncorroded microstructures

The microstructure of a refractory system, be it brick or monolithic, is composed of large, discrete aggregate, filler or grain particles held together by a bond or matrix phase.[9] In the present study the microstructures of all uncorroded bricks from the back face of the slag test samples were similar, revealing light tabular alumina and spinel grains with a darker, porous bond phase (Fig. 1). At higher magnification (Fig. 2) the tabular grain is shown to contain small (1–5 μm) pores with some angular grain pull-out. EDS of the tabular alumina showed only Al, whereas the spinel showed Al and Mg levels consistent with the proportion expected for each spinel type. It proved difficult to distinguish spinel from alumina since both have similar weighted average atomic numbers (so atomic number contrast is similar) and the high Al_2O_3 content of the spinels renders their contrast even more like that of pure alumina. However, characteristic bright phases occurred at triple junctions in the sintered spinel (Fig. 3), enabling them to be distinguished from the tabular alumina. The triple junction phase contained Al, Ca, Mg and Na. X-ray dot mapping of Mg in the 67% alumina spinel (MgO-rich) revealed small (several μm) Mg-rich regions which appear to be periclase precipitated within spinel grains. The bond phase linking the alumina and spinel grain is more complex, containing facetted light grey tabular alumina fines, black pores, spinel fines and other phases (Fig. 1). Detailed analysis of the bond shown at higher magnification in secondary and backscattered electron modes in Fig. 4 reveals the fine (μm) spinel and alumina particles. These particles are embedded in a porous matrix the individual phases of which could not be identified; it is possible much of it has been removed or contaminated during polishing.

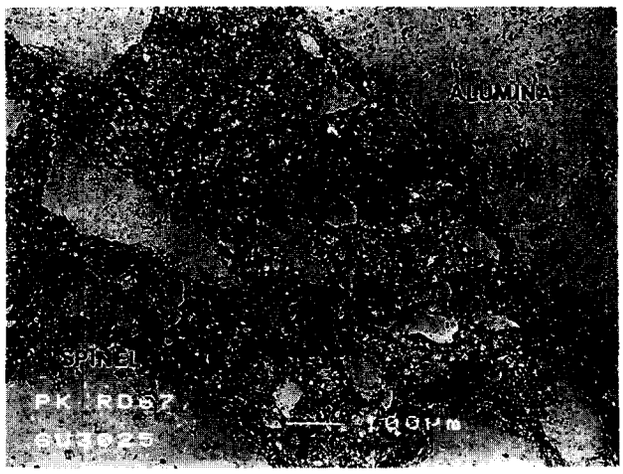

Fig. 1. Backscattered electron image of 67% Al_2O_3 spinel alumina sample away from the corrosion front, showing the tabular alumina and spinel grains and the complex bond.

Fig. 2. Secondary electron SEM image of a tabular alumina grain well away from the corrosion front, showing its porous nature.

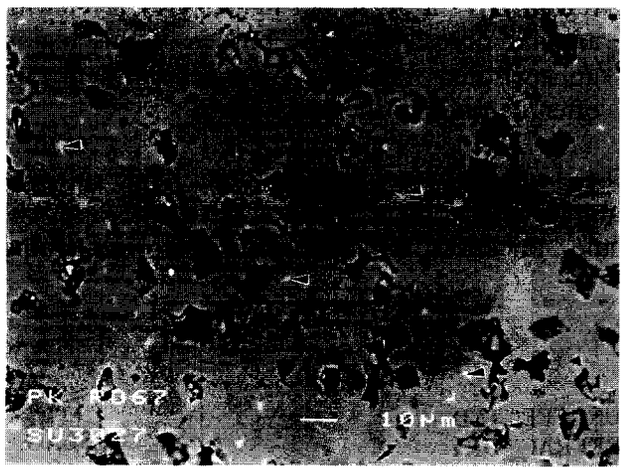

Fig. 3. Characteristic bright phases (arrowed) at triple junctions of the sintered spinel grains.

3.2 Corroded microstructures

The microstructure of the corroded samples consists of a slag layer still attached to the castable surface and a dense layer behind the slag further into the refractory which can be separated into two main regions. These are (Fig. 5):

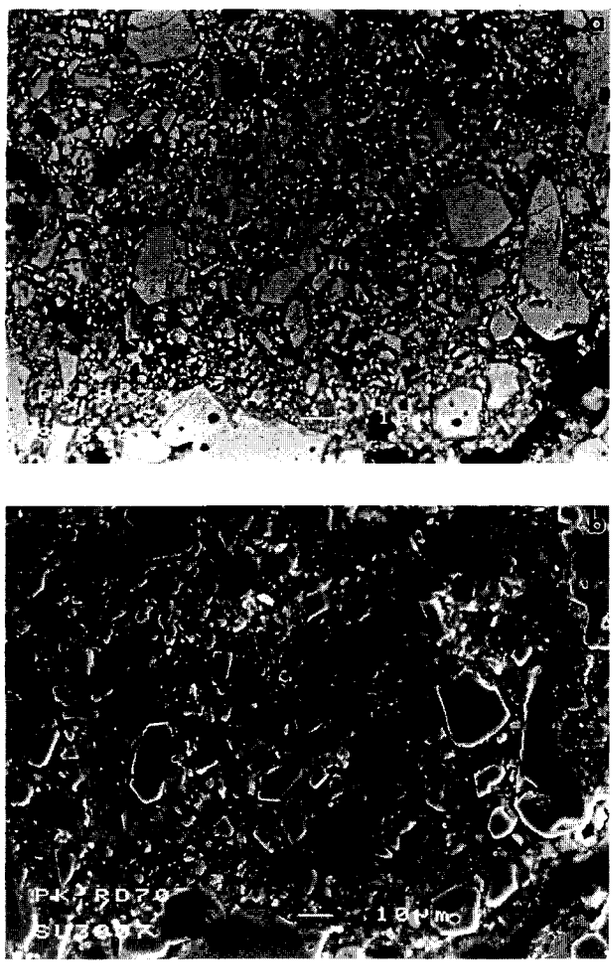

Fig. 4. Secondary and backscattered electron images of the bond phase in an uncorroded part of a 70% Al_2O_3 spinel–alumina sample.

region I — a dark penetrated layer containing tabular crystals in a glass matrix. The density of this layer is highest at the interface with the slag; and

region II — a dense but lighter grey layer with angular pores. Near the border of this region unpenetrated refractory needles/whiskers are often detected in the bond phase.

These regions were more distinguishable in some samples than others. Table 4 gives the approximate thickness of the slag layer remaining

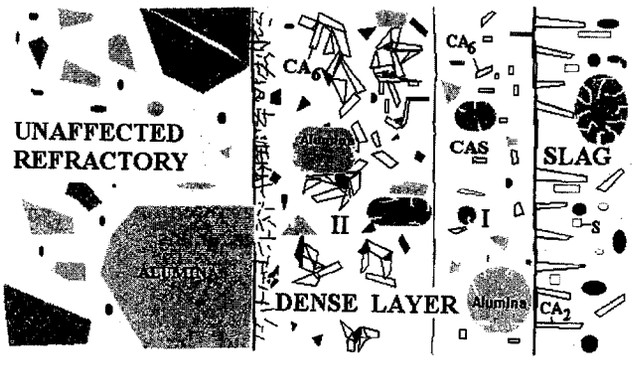

Fig. 5. Schematic diagram (not to scale) of the general form of the penetration front.

Table 4. Erosion and slag penetration depth and thickness of remnant slag

Spinel type (wt% Al_2O_3)	*Average erosion (mm)*	*Average slag penetration (mm)*	*Thickness of remnant slag layer (mm)*
67	7·7	0	2·05
70	10·3	0	1·1
75	12·8	0	1·18
90	12·5	2·0	1·0
No spinel	11·2	5·6	1·05

attached to the refractory sample, although it should be noted that this thickness was variable along the length of each sample. Apart from the spinel with 67% alumina, which is about twice the thickness of the others, the differences are small.

Detailed analysis of the phases present in the penetrated refractories will now be presented. Figure 6 shows the slag layer from the 67% sample containing many phases and most of the Fe from the original slag composition. The main slag phases are revealed at higher magnification (Fig. 7) to be a dark grey angular phase and grey elongated grains in a matrix of light grey grains with white intergranular phase. EDS shows the dark grey angular phase to contain Mg, Mn, Fe, Al and O with a mole ratio of 1 (MgO/MnO/FeO) to 2 Al_2O_3, indicating it is a highly aluminous impure spinel labelled S in Fig. 7. Other grains of similar composition often occurring in penetrated 'clumps' (also labelled S in Fig. 6) are spinel grains eroded from the castable surface and gradually reacting with the slag. Note the thermal expansion cracks around the spinel clump. The lighter grey needles are a calcium aluminate with a Ca/Al

Fig. 6. Secondary electron SEM image of the attached slag/refractory interface of a 67% Al_2O_3 spinel–alumina sample. S is a detached spinel grain. Note that the CA_2 crystals are perpendicular to the refractory surface until about halfway across the slag layer when they become more randomly oriented.

Fig. 7. Detail of the slag phases showing CA_2 needles, blocky spinel (S), calcium aluminosilicate (CAS) matrix and bright phase G whose triple junction morphology suggests it is the last phase remaining after crystallization and may well be glass.

Fig. 9. Detail of the CA_6 crystals in a CAS matrix.

atomic ratio of 1:4·3. These are $CaO.2Al_2O_3$ but rich in alumina (labelled CA_2 in Fig. 7). The light/dark grey matrix grains are various calcium aluminosilicates with an approximate mole ratio of 6·2:4:2·4 $CaO/Al_2O_3/SiO_2$ (labelled CAS). The white phase has variable composition but is usually rich in CaO + Al_2O_3 (60 wt%) and MnO + FeO (40 wt%). This phase is probably uncrystallized glass (labelled G). Note the columnar nature of the CA_2 slag grains growing perpendicular to the refractory interface (Fig. 6), suggesting rapid undisturbed growth until about half way into the slag layer when more random crystal orientation occurs. The latter indicates that either (1) crystals were moving in the slag stream or (2) nucleation and growth was more random.

Region I (illustrated in Figs 8 and 9 for 75% spinel) in the dense layer contains tabular crystals of about 1:7 CaO/Al_2O_3 mole ratio. These are most likely alumina-rich calcium hexaluminate $CaO.6Al_2O_3$ (labelled CA_6) whereas region II (illustrated in Fig. 10 for 75% spinel) has similar grains but separated by angular pores. Similar facetted CA_6 crystals have been observed in corroded alumina–spinel refractories.[1] The matrix in regions I and II contains CaO, Al_2O_3 and SiO_2 (CAS) but the composition is variable. This type of matrix was never observed either in the uncorroded parts of the refractories or in uncorroded sections held for 40 h at 1650°C and its presence suggests extensive CaO and SiO_2 penetration; near the slag layer MnO and FeO were detected. Region II close to the unpenetrated refractory contains a large number of needles or whiskers (illustrated in Fig. 11 for 75% spinel) suggesting vapour involvement in their deposition. The needles/whiskers are mostly alumina with some CaO, so they are also alumina-rich CA_6.

A final significant observation is that the growth of the elongated CA_2 grains in the slag is less clearly perpendicular to the refractory in all samples other than the 67% spinel sample (e.g. Fig. 12 for the no spinel sample).

Fig. 8. Tabular CA_6 crystals in dense region I at the slag/refractory interface of a 75% Al_2O_3 spinel–alumina sample.

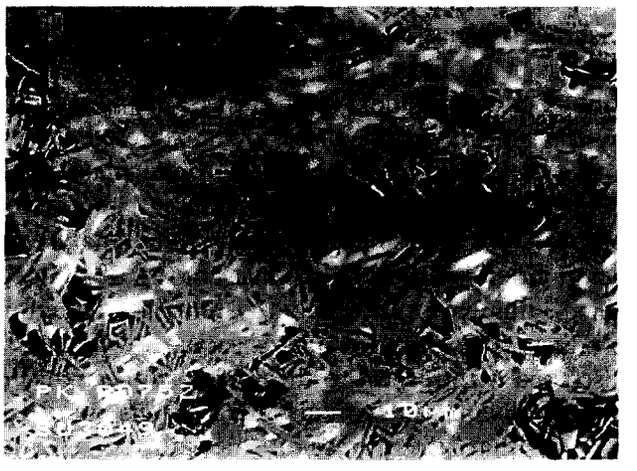

Fig. 10. CA_6 crystals from the same sample as in Fig. 8 in porous region II.

Fig. 11. CA_6 whiskers/needles close to the unaffected refractory from the same sample as in Fig. 8.

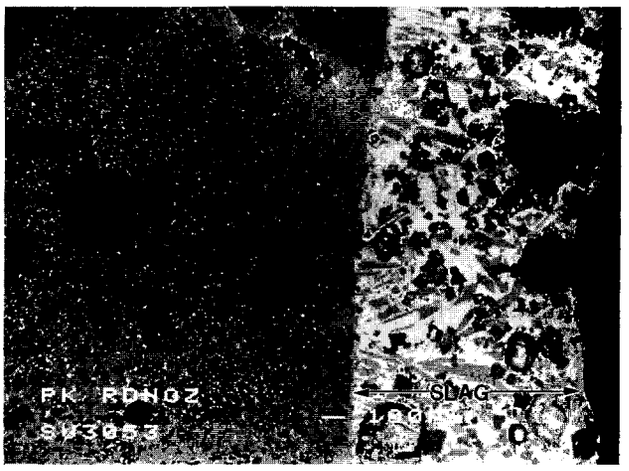

Fig. 12. More random distribution of CA_2 crystals throughout the attached slag in the no spinel sample.

4 Discussion

The microstructural analysis revealed no great differences between the microstructures of the various stoichiometry spinel samples, either of the uncorroded samples from the back face of the castable blocks or the corroded castables near the slag. Uncorroded microstructures contained the tabular alumina and spinel grains, distinguishable by the bright second phase in the sintered spinel, and a complex bond phase. This bond phase contained spinel and alumina fines but the other phases were too small to resolve and analyse in detail (Fig. 4) although it must consist of the calcined alumina and calcium aluminate reaction products. The corroded microstructures will now be discussed with respect to the corrosion mechanism.

Several Japanese workers, e.g. see Refs 7 and 10, suggest that the corrosion mechanism of alumina–spinel refractories by a $CaO–MnO–Al_2O_3–FeO/Fe_2O_3–SiO_2$ slag is relatively simple. The CaO in the slag reacts with alumina in the refractory so that the slag becomes alumina-rich and precipitates low melting CA_2 and CA_6 products at the hot face. The refractory spinel, however, reacts with the slag MnO and FeO/Fe_2O_3 forming complex spinels, i.e. $(Mg, Mn, Fe)O.(Fe, Al)_2O_3$. Deeper into the refractory, as the CaO and Al_2O_3 are used up forming CA_2 and CA_6 phases, the relative amount of silica increases to generate a high viscosity and high melting temperature slag which limits slag penetration.[11] Gehlenite (C_2AS) is often seen deeper into the refractory, arising from reaction of the CA_2 with silica from the slag. The observations of corroded microstructures in this study are in general agreement with this model.

The general corrosion mechanism will initially involve reactions with the matrix fines followed by attack and dissolution of the aggregate grains. Fluid (lime-rich) slag penetrates along the porous bond phases and reacts with the low melting (CA cement reaction products) and finer spinel and alumina fractions to give a CaO- and alumina-saturated slag. Erosion of some grain will also occur at this stage and the Mn and Fe find their way into the spinel (Fig. 6). Recrystallization of CA_2 and CAS occurs in the slag and CA_6 in the corroded castable (region I). Vapour produced from these reactions may penetrate into the castable, opening up the microstructure and allowing further penetration of liquid. The slag becomes more viscous deeper into the brick as its composition becomes more silica-rich and the reaction rate slows. On cooling the slag contains the elongated CA_2 grains, spinel crystals, calcium aluminosilicate phase and remnant Mn- and Fe-rich glass. The CAS phase probably contains gehlenite (C_2AS) as observed by Mori *et al.*[8] and Kurata *et al.*[10] The viscous slag within the refractory precipitates the alumina-rich CA_6 angular crystals from the liquid (region I) and these crystals are also present in region II although there is less liquid here and angular pores remain. Further into the refractory the CaO and Al_2O_3 have reacted to form alumina-rich CA_6 whiskers. While it is impossible to say whether a vapour phase was involved in their formation, whiskers are commonly formed via a vapour-phase reaction.[9] Sato *et al.*[12] examined rotary slag corrosion of a similar composition alumina–spinel castable by a similar slag and used X-ray diffraction (XRD) to determine the phase composition as a function of distance into the corroded refractory. They found Al_2O_3, CA_6 and CA_2 near the slag/refractory interface, then Al_2O_3, spinel, CA_6 and CA_2, followed by Al_2O_3, spinel and CA_6 at the most penetrated regions, consistent with the present study.

The benefit of alumina-rich spinel in improving the corrosion resistance of alumina–spinel refractories has been well documented.[4,5] This improvement is thought to be due to the fact that alumina-rich spinels contain an excess of charge compensating cation vacancies on octahedral sites.[13] Consequently, it is easier for the cations in the slag to find their way into these vacancies, so that the increased viscosity and melting temperature of the slag associated with higher SiO_2 content is achieved earlier in the corrosion process.[4] While there have been several studies of corrosion of alumina-rich spinels by steel slags, there appears to be little data on MgO-rich spinels. However, the MgO-rich spinel had the best erosion resistance in the present study and the reasons for this behaviour need to be considered. Examination of the MgO– Al_2O_3 binary phase diagram reveals that a 67% alumina spinel (as used in the present study) would contain excess MgO. In fact, periclase is revealed in XRD scans of the MgO-rich spinel.[14] Consequently, corrosion of this spinel by the slag would release excess MgO. The factors having most influence on the slag viscosity are temperature and composition. Assuming that the temperature was constant for all samples since they were tested simultaneously, composition is the variable of interest. The MgO content of a CMAS slag is known to have a critical effect on the corrosion rate of alumina.[15] The higher the MgO content, the lower the dissolution rate of alumina. From this respect the corrosion test results are not surprising since the lower alumina spinels (such as 67%) would eventually dissolve more MgO into the slag, allowing less local dissolution of the alumina. Often a crystalline spinel layer forms in the slag close to the alumina[16] which acts to protect the alumina from further attack, the dissolution rate of spinel in a CMAS slag being much lower than alumina (as evidenced by the clumps of spinel grain remaining in the slag, Fig. 6). No such protective spinel layers were observed here, perhaps because the overall MgO content of the slag was too low.

The most obvious difference between the different alumina spinels in the present study was the much thicker slag layer on the least corroded refractory (67% spinel, Table 4). The 67% sample also showed columnar growth of CA_2 crystals from the interface, suggesting a highly viscous layer of slag was at the refractory interface, but further away from the castable the movement of the slag was greater and crystallization more random (Fig. 6). The other samples did not show this behaviour and had thinner, less columnar, slag layers at the refractory interface suggesting more fluid slag being present (Fig. 12), consistent with the argument presented above.

Mori *et al.*[8] used a slag of similar composition to corrode alumina–stoichiometric spinel refractories and found that the spinel-free samples had the highest Fe_2O_3 discoloration as was observed in this study (Table 4). This was attributed to the fact that spinel can take FeO/Fe_2O_3 in solid solution and so reduce the discoloration in spinel-containing samples, an explanation which may also apply here. Note, however, that slag penetration will be greater than the depth of the discoloured region.[8]

5 Conclusions

Uncorroded alumina–spinel refractories contain the phases expected in the microstructure, i.e. tabular alumina and sintered spinel grains bonded by a porous matrix containing fines of spinel, alumina and calcium aluminates.

The corroded microstructure contains several regions. The attached slag comprises needle-like CA_2 crystals, partly corroded spinel grain, small (<30 μm) facetted spinel crystals, calcium aluminosilicate phases and remnant (possibly glassy) Ca/Al/Mn/Fe oxide. Deeper into the refractory is a dense layer (region I) of tabular CA_6 crystals in a CAS matrix and even deeper is a region of similar CA_6 crystals but with angular pores present and a CAS matrix (region II). Near the border of this phase with unaffected refractory are needles/whiskers of CA_6, suggesting a vapour-phase reaction may be occurring.

This microstructure is consistent with the previously suggested corrosion mechanism although providing more detail of the process. The corrosion involves initial reaction of CaO in the slag with alumina fines in the refractory bond. The slag becomes saturated in CaO and Al_2O_3, and CA_2 is precipitated from it along with other calcium aluminosilicates. The spinel fines and grain in the refractory take up the $MnO/FeO/Fe_2O_3$ from the slag, which becomes silica-rich as CA_2 is precipitated and highly viscous. The thickness of the remnant slag layer on the corroded samples indicates the viscosity of the liquid slag under the test conditions and may prove a valuable indicator in post-mortem analysis of corroded microstructures. Further into the refractory CA_6 is formed, firstly crystallized with a tabular morphology in dense regions and then with a similar morphology in more porous regions. Deeper still in the refractory CA_6 takes a whisker/needle habit suggesting some vapour-phase reaction.

MgO-rich spinel–alumina castables undergo less corrosion under these conditions as dissolution of MgO leads to a viscous MgO-rich slag which is less corrosive to the Al_2O_3 component of the refractory.

Acknowledgements

The rotary slag testing was carried out at British Steel Teesside Technology Centre. We would like to thank Dr Mark Warman at that centre for useful discussions.

References

1. Mori, J., Watanabe, W., Yoshimura, M., Oguchi, Y. & Kawakami, T., Material design of monolithic refractories for steel ladle. *Bull. Am. Ceram. Soc.*, **69**(7) (1990) 1172–1176.
2. Nagai, B., Matsumoto, O. & Isobe, T., Development of monolithic refractory linings for BOF ladle in Japan mainly for the last decade. *Proc. UniteCR 91*, **2** (1991) 116–122.
3. Yamamura, T., Hamazaki, Y., Kaneshige, T., Toyoda, T., Nishi, M. & Kato, H., Alumina–spinel castable refractories for steel teeming ladle. *Taikabutsu Overseas* **12**(1) (1992) 21–27.
4. Sumimura, H., Yamamura, T., Kubota, Y. & Kaneshige, T., Study on slag penetration of alumina–spinel castable. *Proc. UniteCR 91*, **2** (1991) 138–144.
5. Fujii, K., Furusato, I. & Takita, I., Composition of spinel clinker for teeming ladle casting materials. *Taikabutsu Overseas*, **12**(1) (1992) 4–9.
6. Vance, M. W., Kriechbaum, G. W., Henrichsen, R. A., Maczura, G., Moody, K. J. & Munding, S., Influence of spinel additives on high alumina/spinel castables. *Bull. Am. Ceram. Soc.*, **73**(11) (1994) 70–74.
7. Matsumoto, O., Isobe, T., Nishitani, T. & Genba, T., Alumina–spinel monolithic refractories. US Patent 4 990 475, 1991.
8. Mori, J., Yoshimura, M., Oguchi, Y., Kawakami, T. & Ohishi, I., Effect of slag composition on wear of alumina–spinel castable for steel ladle. *Taikabutsu Overseas*, **12**(1) (1992) 40–45.
9. Lee, W. E. & Rainforth, W. M., *Ceramic Microstructures Property Control by Processing*. Chapman and Hall, London, UK, 1994.
10. Kurata, K., Matsui, T. & Sakaki, S., Castable lining technique to bottom of teeming ladle. *Taikabutsu Overseas* **12**(1) (1992) 29–39.
11. Nagai, B., Matsumoto, O., Isobe, T. & Nishiumi, Y., Wear mechanism of castable for steel ladle by slag. *Taikabutsu Overseas*, **12**(1) (1992) 15–20.
12. Sato, Y., Joguchi, H. & Hiroki, N., Test results of alumina–spinel castable for steel ladle. *Taikabutsu Overseas*, **12**(1) (1992) 10–14.
13. Dupree, R., Lewis, M. H. & Smith, M. E., A study of the vacancy distribution in non-stoichiometric spinels by magic angle spinning NMR. *Phil. Mag.*, **A53** (1986) L17–L20.
14. Wilson, D. R., Evans, R. M., Wadsworth, I. & Cawley, J., Properties and applications of sintered magnesia–alumina spinels. *Proc. UniteCR 93* (1993) 749–760.
15. Sandhage, K. H. & Yurek, G. J., Direct and indirect dissolution of sapphire in calcia–magnesia–alumina–silica melts: dissolution kinetics. *J. Am. Ceram. Soc.*, **73**(12) (1990) 3633–3642.
16. Herzog, S. P., On the formation of protective spinel layers on refractories. *Scand. J. Metall.*, **5** (1976) 145–150.